Journal of Applied Electrochemistry (2007) 37:161–171
DOI 10.1007/s10800-006-9229-5

Electrical and thermal investigation of a self-breathing fuel cell

S. SAILLER[1], S. ROSINI[1], M.A. CHAIB[1], J.-Y. VOYANT[2], Y. BULTEL[1,*], F. DRUART[1] and P. OZIL[1]
[1]*Laboratoire d'Electrochimie et de Physico-chimie des Matériaux et des Interfaces, UMR 5631 CNRS-INPG-UJF, BP 46 Saint Martin d'Hères, 38402, France*
[2]*Laboratoire d'Electrotechnique de Grenoble, UMR 5529 CNRS-INPG-UJF, BP 46 Saint Martin d'Hères, 38402, France*
*(*author for correspondence, tel.: + 33-476-82-65-80, fax: + 33-476-82-67-77, e-mail: Yann.Bultel@lepmi.inpg.fr)*

Received 14 February 2006; accepted in revised form 23 August 2006

Key words: current distribution, impedance, magnetic field, self-breathing PEMFC, temperature distribution

Abstract

This study presents a new method of PEMFC characterisation carried out experimentally on a self-breathing fuel cell from PaxiTech® (25 cm^2 electrode surface area). First, dc and ac measurements were performed on this cell on the basis of models originally dedicated to a Gas Diffusion Cathode. Electrochemical Impedance Spectroscopy (EIS) measurements were performed to characterise the general electrical behaviour of the cell. This technique is of particular interest for improving our understanding of mass transport limitations in PEMFCs. Second, current and temperature distributions over the fuel cell area were determined. Measurements of the locally induced magnetic field and the temperature then provided an indirect evaluation of the current densities in the fuel cell. Both methods were used to determine heterogeneous current density distributions and showed that the highest current densities were close to the current collectors.

1. Introduction

Miniaturised fuel cells are potentially beneficial as a replacement or supplement for batteries. For fuel cells to be successfully integrated into electrical appliances their dimensions must be fitted to the existing geometry of the device. The ideal planar design consists of an open cathode side to allow passive, full self-breathing operation of the fuel cell. An important advantage of the open cathode is that additional ventilation by fans is not needed.

The development of such Polymer Electrolyte Membrane Fuel Cells (PEMFC) for portable applications requires electrodes with a high power density for a small catalyst loading. PEMFCs should be able to operate at high current density and with acceptable efficiency. Losses inherent to high current densities are due to ohmic losses and slow oxygen diffusion to the cathode when using air. The latter adds to the limited interfacial kinetics of the Oxygen Reduction Reaction (ORR) within the cathode active layer. It is well established that a high performance electrode must offer good gas access to electrocatalyst particles in the active layer. Nevertheless, outside the active layer, slow diffusion in the gas phase can lead to oxygen depletion. Some experimental studies have highlighted the influence of the gas-diffusion layer on PEMFC performance [1].

Electrochemical impedance spectroscopy (EIS) appears to be particularly useful for providing a better understanding of mass transport limitations in PEMFCs [2]. Recently, impedance techniques were used to investigate the response of complete single cells [3]. One of the main findings of these studies concerned the important role of water transport in the membrane and of oxygen diffusion in the gas diffusion layer of the electrode. Freire and Gonzales [4] studied the impedance response of H_2/O_2 PEMFC in different working conditions and with different membrane thicknesses. Their results clearly showed that thinner membranes present better characteristics for water management. Moreover, local temperature measurements in the electrodes tend to show that current distributions may be non-uniform, especially in large cells [5]. Some techniques have already been described to determine current density distribution [6]. One technique involves placing several electrically isolated subcells within the Membrane Electrode Assembly (MEA). These subcells provide information about the electrochemical activity in the fuel cell. A second method is current distribution mapping [7] using a passive resistor network distributed throughout the MEA. A third method [8] uses Hall-effect current sensors with magnetic tores inserted in the collector plate for each cell.

Experiments have shown that self-breathing PEMFC performance depends on oxygen diffusion in the different cathodic regions and the location of the current collector. In the present study, DC and AC measurements were performed on the basis of models originally dedicated to a Gas Diffusion Cathode. These models include mass transport limitation in the gas diffusion. The electrochemical measurements provided the overall response of the 25 cm^2 PEMFC. An indirect evaluation of the current densities over the fuel cell area was then obtained by measuring the locally induced magnetic field. Temperature distribution was also recorded by using thermocouples and an infrared camera, which are powerful techniques because they allow thorough investigation of the whole electrode area. This distribution showed the influence of the geometric parameters: cell design and position of the current collector.

2. Experimental

The electrochemical fuel cell under study was a 25 cm^2 self-breathing single cell produced by PaxiTech® (http://www.paxitech.com) for laboratory experiments in accordance with our particular specifications for magnetic measurements. As shown in Figure 1, the fuel cell comprises an air breathing cathodic compartment, an MEA (Membrane Electrode Assembly) and a standard anodic compartment. Since it is a self-breathing cell, the cathodic side has a plate with holes to allow air access to the MEA. However, the anodic compartment is fed with hydrogen at approximately 1.2 bars and is equipped with a porous diffusive plate to enable hydrogen to diffuse to the MEA.

The MEA is composed of 7 layers: 2 dissymmetric gaskets, 2 gas diffusion layers, 2 catalytic layers and a Nafion®-112 membrane. The diffusion layer is composed of carbon fiber-based non-woven felts of 200 μm thickness. Two types of MEA were used: one with two catalytic layer loadings of 0.3 mg platinum/cm^2 and the other with two catalytic layer loadings of 0.8 mg platinum/cm^2. Copper grid collectors were placed on each side of the MEA to collect current over the 25 cm^2 electrode area. They were kept in contact with the terminal collector at the edge of gas compartment.

2.1. *Electrochemical measurements*

Polarisation curves were recorded using a Solartron 1286 electrochemical interface. In order to obtain stationary states, the fuel cell was maintained for 1 h under a 0.5–1 A current before starting the polarisation experiments. All the stationary points on the polarisation curves were recorded for 1 min. Only one point could be used to collect current and connect the measuring device. Consequently, the measured cell voltage included part of the ohmic drop in the collector so that the fuel cell potential was thus underestimated.

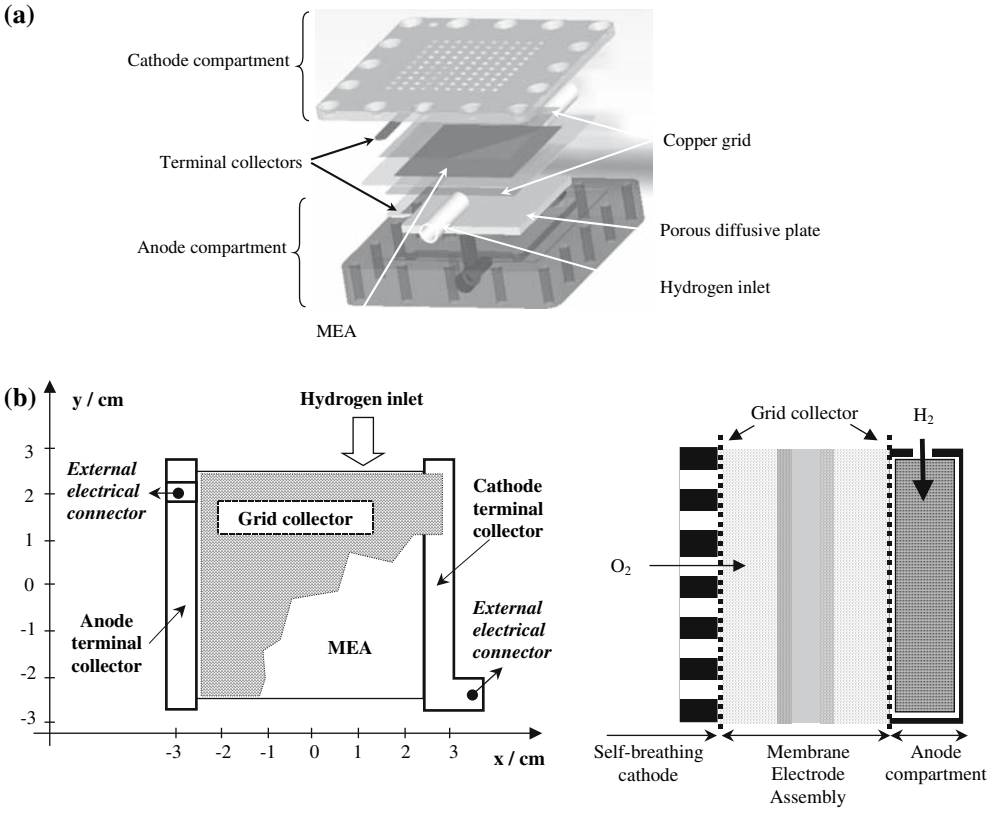

Fig. 1. (a) Element of the self-breathing PEM fuel cell from PaxiTech®. (b) Schematic representation of the Membrane Electrode Assembly with current collectors.

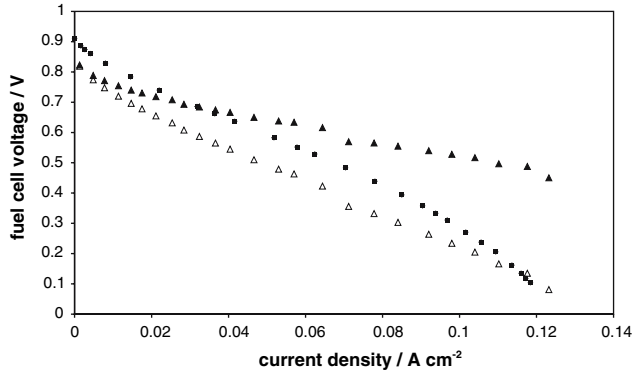

Fig. 2. Polarisation curves of a self-breathing PEM fuel cell (T = 30 °C, P_a = 1.2 bar, P_c = 1 bar): Influence of the catalyst loading △: 0.3 mg cm^{-2} (▲: cell voltage corrected from the IR drop) and ■: 0.8 mg cm^{-2}.

On the basis of the experimental cell resistance obtained from the impedance measurement (see Figure 3), the cell voltage values were corrected for ohmic drop and is also shown in Figure 2. Electrochemical impedance was recorded at frequencies between 0.1 and 65,000 Hz with a 50 mV oscillation amplitude using a Solartron 1250 frequency response analyser with the above-mentioned Solartron 1286 electrochemical interface.

2.2. *Magnetic measurement*

Local cell activity and related current sourcing were evaluated by measuring the instantaneous magnetic field as close as possible to the MEA (Figure 1(b)). This indirect method is non-intrusive and avoids any modification of the cell structure and response. DC magnetic induction was measured over the entire cell surface and presented in the form of a matrix for each pair of coordinates (x,y).

The magnetic sensors were selected for their ability to cover the magnetic range of the induced fields. A first approach to sensor sizing is given by Ampere's law (Equation 1).

$$\oint Hdl = \sum i \tag{1}$$

In the present cell, virtually all ferromagnetic materials were removed. Induction and magnetic fields are therefore ideally linked by the magnetic permeability of free space with $\mu_0 = 4\pi 10^{-7}$. The maximum value of the rotational induction field B_{max} (see Figure 11(a) for example) is reached along the outer perimeter of the active cell area. Equation 2 offers a practical way of approximating this value using the rated value of the cell current I and assuming a circular induction path on a diameter ∅ equal to the cell size, which enables the calculations to be simplified by separating the integrals:

$$B_{max} = \frac{\mu_0 I}{\pi \cdot \phi} \tag{2}$$

In this case, the specific values were: I = 4 A, ∅ = 5 cm and B_{max} = 32 μT.

The magnetic sensor must be very sensitive and accurate. To meet our constraints we chose two-axis magneto-resistive probes (i.e. HMC 1022) with a maximum range of ± 600 μT and a sensitivity of 10 V/V/T. The sensor electrical output was amplified using common electronic circuits and then directly converted into a digital response for further calculations. Matlab® mathematical software was used to compute the current density distribution.

In practice, the value of induction B_{max} obtained from equation 2 has to be considered in light of the following hypotheses:

- Current density may not be uniform and magnetic induction may be locally higher depending on activity in the immediate vicinity.
- Current collectors and incoming feeders may also increase the measured fields. These unexpected fields can be ignored by simple modelling using their specific characteristics (symmetries and axis orientations). However, it must be verified that the probes are not saturated by these additional fields. The effects can be reduced when the electrical connections – outside the cell – are straight and are kept in the cell plane.
- The magnetic field of the earth (≈60 μT) determines the absolute and optimum cell orientation: the influence of this superimposed field is less when the cell plane is located perpendicularly to it (north direction with approximately 60° inclination from horizontal at our latitude). It is necessary to check again that this additional field does not saturate the probes.
- Special care has to be taken to keep the probe perpendicular to the cell while moving the sensor above the cell surface and in line with the x and y axes. A mechanical system must be used to keep the probe at a constant orientation in relation to the cell while moving it in parallel with the cell surface and measuring the induction at different points.

A first evaluation of local density can be computed using Maxwell's equations. This evaluation assumes that the induction measured in the immediate proximity of the membrane is similar to the field in the membrane thickness because B is continuous (Equation 3) and the sensor (coordinate z_1 = 5 mm) is just above the membrane plane (coordinate z = 0).

$$\mathrm{div}\vec{\mathrm{B}} = 0 \tag{3}$$

Then the local current density J in the membrane is given by Equation 4 [8] where J depends only on the variations in induction B along the x and y axes:

$$\vec{\mathrm{J}} = \frac{1}{\mu_0}\,\mathrm{r\vec{o}t}\,\vec{\mathrm{B}} \tag{4}$$

This equation shows that the superimposed earth field has no effect on the computed current values because it is constant over the cell surface.

A more accurate evaluation of the field induced near the cell is given by Biot & Savart's law from Equation 5. In this case, all the current sources, the electrode thickness and the sensor coordinate z_1 can be taken into account.

$$\vec{B} = \iiint \frac{\mu_0 \vec{J} \times \vec{\hat{r}}}{4\pi r^2} dv \quad (5)$$

where $\vec{\hat{r}}$ is the unit vector for the distance r from the current to the field point. This equation is useful for analysing the complete configuration of the cell electrical outputs. But inverse calculation of local density J from B is not easy. Some indications for inverse methods may be found in Ref. [9]. In this case, the currents could have been evaluated with greater accuracy if 3-axis induction measurements had been used.

2.3. *Temperature measurement*

Two different techniques were used to measure temperature on the self-breathing fuel cell. First, nine K thermocouples were placed in contact with the cathode and temperatures were recorded along a polarisation curve using a Keithley 2000 multimeter controlled by in-house software. As previously, in order to obtain stable fuel cell performance, polarisation and temperatures were recorded in the same conditions as for the previous electrochemical measurements.

In order to confirm temperature changes and distribution, the temperature field was recorded using an infra-red camera driven by ThermoScan software.

3. Results

Figure 2 shows two different polarisation curves obtained for fuel cells with respective platinum electrode loadings of 0.3 and 0.8 mg per cm^2. For both cells, the open circuit potential was lower than the thermodynamic value, which is in agreement with the literature. Classically, such a result is explained by the non-equilibrium of the oxygen reaction at the cathode. However, the particularly low open circuit voltage in the present cell could be due to a partial leakage of hydrogen. For low current, a significant decrease in voltage vs. current was observed due to electrochemical activation phenomena. For a medium current, voltage decreased linearly with current. Finally, for a high current density, the shape of the polarisation curve indicates a possible mass transport limitation. It is worth mentioning that performances were similar at very low cell potential where fuel cell behaviour was controlled by the oxygen diffusion process at the cathode. As show in Figure 2, the catalyst loading had no influence on the overall shape of the polarisation curve but a platinum ratio increase clearly improved the electrochemical performance of the fuel cell, as expected.

Figure 3 shows a characteristic impedance diagrams (Nyquist and Bode plots) obtained along the polarisation curve with 0.3 mg per cm^2 of platinum in the electrodes. At high frequency, the impedance diagram shows an inductive part represented by a line parallel to the imaginary axis and shifted toward positive real values. This behaviour is attributed to the contribution of the electrical connections, which masks the charge transport phenomena in the electrolyte and a part of high frequency interface response. Nevertheless, the electrolyte resistance can be evaluated by measuring the high frequency intersection of the impedance diagram with the real axis. The capacitive loop recorded between 1000 and 0.1 Hz is characteristic of the contribution of self-breathing fuel cell interfaces to impedance. A first approach in the development of the model involved identifying this loop using an electrical model [10]. The impedance diagram seemed to be composed of two different depressed semi-circles, characterised by two distributed capacities in parallel with two resistances, in series with an inductive contribution, as shown in Figure 3(a). Given this electrical fit, the two separate arcs could not be attributed to physical phenomena such as anode and cathode contributions or mass transport limitations and electrochemical kinetics. Changes in the experimental impedance diagram with polarisation are plotted in Figure 3(b). In agreement with the polarisation measurements, an overall decrease in impedance was observed with polarisation. As previously, variations in the impedance diagram can be described as a function of frequency. For a high frequency, a small decrease in the real part of the impedance was observed. Such a decrease may be related to increased electrolyte conductivity due to partial humidification of the polymer membrane. A straight line at a 45° angle appears in the high frequency limit. This is attributed to distributed resistance in the electrode [11, 12]. This behaviour can be ascribed to double layer charging and ionic transport through the active layer, which dominate the overall electrode response for high frequencies in the case of low ionic conductivity. The low frequency depressed arc decreases with polarisation and can thus be linked to the contribution of electrochemical kinetics [13]. Finally, an additional and not well-defined contribution appears in the low frequency domain, increasing with polarisation.

In order to obtain the current density distribution over the cathode, the magnetic field was measured near the self-breathing side of the fuel cell. Measured projections Bx and By of the magnetic field vector – respectively along the x and y axes – are shown in Figure 4(a, b) for two different currents. The magnetic fields were measured both when current was flowing through the fuel cell and when the fuel cell was under open circuit voltage. Comparison of these magnetic fields clearly shows that currents on the breathing side of fuel cell induced a variation in magnetic field. This result was confirmed by the increase in the magnetic field value

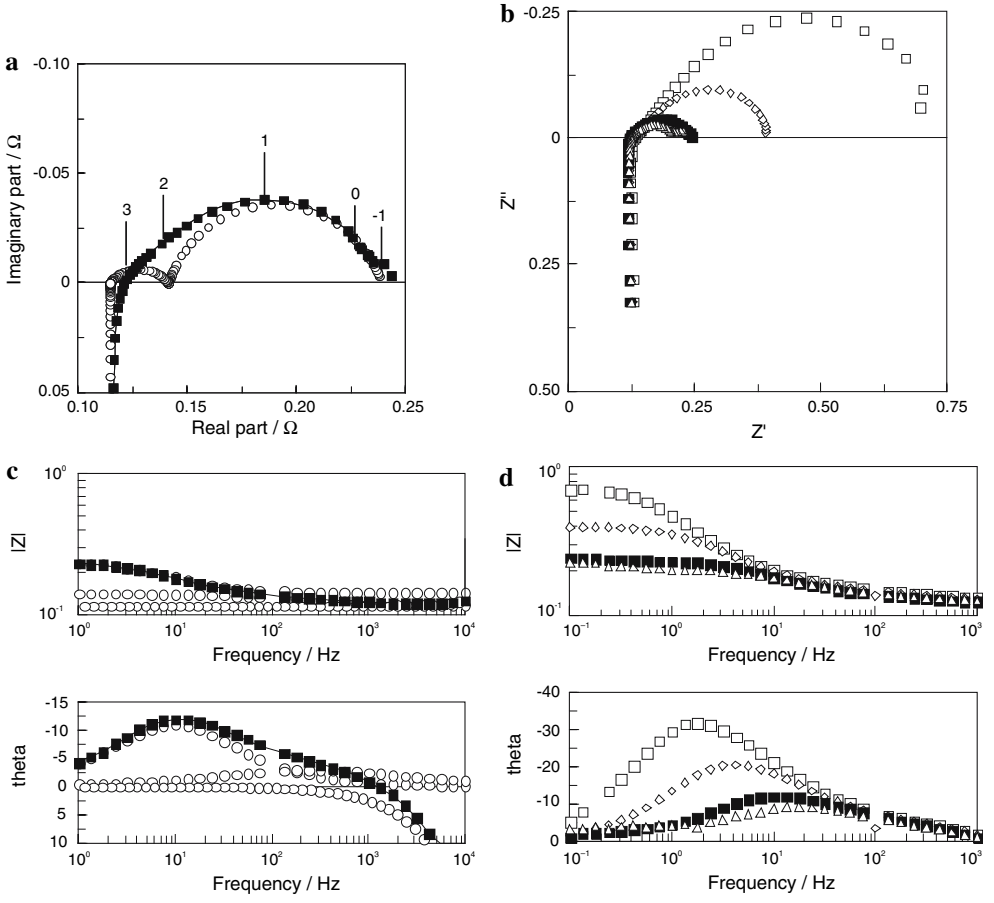

Fig. 3. (a, c) Example of impedance fitting with an electrical model. ■: Experimental data; line: results obtained with electrical model; ○: evaluation of each separate contributions of electrical model; (b, d) evolution of impedance (□: 0.033 A–0.8 V; ◇: 0.155 A–0.74 V; ■: 0.8 A–0.560 V; △: 1.60 A–0.38 V) with cell polarisation of a self-breathing PEM fuel cell (T = 30 °C, P_a = 1.2 bar, P_c = 1 bar) (catalyst loading: 0.3 mg cm^{-2}).

with current density. As shown in this figure, the magnetic fields are not the same along the x and y axes, suggesting a possible heterogeneous distribution of current density due to the geometric configuration of the cell:

– the current flows through the cell along a general x-axis in the anode and cathode collector grids. Therefore it increases the measured induction values along the y-axis (Ampere's law) by adding an almost constant positive induction field to the primary field induced by the current density in the membrane. The measured values of B_y (Figure 4) effectively show a clear tendency towards a positive mean value. Nevertheless, currents in the membrane are still oriented towards the Z-axis and the superimposition of an almost constant field will not interfere with calculations because only differential values of induction are used in the curl term of Equation 4.
– the external electrical connectors of the cell may also cause some local disturbance in the two opposite corners of the fuel cell (see Figure 1(b)).
– the fuel cell is fed with hydrogen gas from a single entry point (see Figure 1b). The gas flows in the cell along a general y-axis. A higher degree of activity is thus expected in this area.

Temperature distribution on the cathode side of the self-breathing fuel cell was also investigated. Figure 5 shows the highest and lowest cell temperatures recorded with nine K thermocouples uniformly distributed over the fuel cell surface and for different fuel cell working conditions. Figure 6 shows the corresponding temperature distribution at low and high current densities. Note that the polarisation curves obtained with thermocouples (Figure 5) and without thermocouples (Figure 2) are similar. Thermocouples therefore do not modify the electrochemical behaviour of the self-breathing fuel cell or of mass transport phenomena occurring at the air cathode. Measured fuel cell temperature increased dramatically with current, due to both the exothermicity of the electrochemical reactions and Joule's law effect. Moreover, as shown in Figure 6, a heterogeneous temperature distribution was recorded on the cathode surface of the self-breathing fuel cell with a temperature gradient of about 2 °C cm^{-1}. Two "hot" regions were observed close to the current collector, while the temperature was lower in the middle of the electrode.

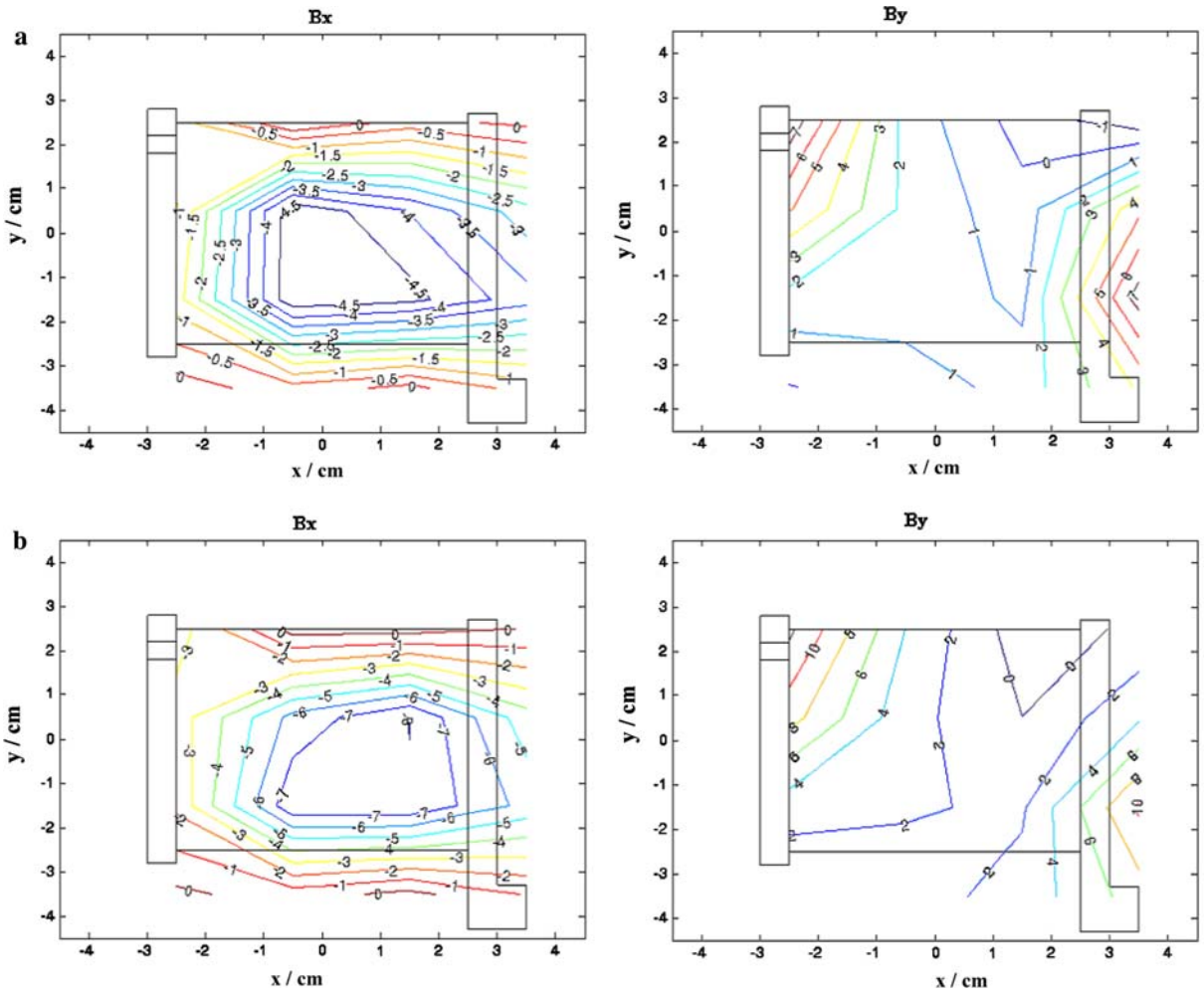

Fig. 4. Magnetic field (μT) recorded near cathode at one polarisation point ((a): 0.06 A cm^{-2} and (b): 0.12 A cm^{-2}) calculated by subtracting the magnetic field recorded with and without current (catalyst loading: 0.3 mg cm^{-2}).

As shown in Figure 6, temperature distribution was not symmetrical, the electrode surface close to the anodic collector being hotter than the surface close the cathodic collector.

4. Discussion

Electrochemical measurements (dc and ac) were analysed using the present model (see annex) in order to extract physical data. This simple model takes in account mass transport at the cathode and electrochemical phenomena. The Tafel slope values for hydrogen (60 mV dec^{-1}) and oxygen (120 mV dec^{-1}) are well-known and thus imposed [14]. In the case of a self-breathing PEMFC, the limiting current is due to oxygen mass transport at the cathode. The magnitude of the limiting current density at the anode is thus assumed to be one order higher than at cathode. The model expresses the cell potential vs. the current density, according to electrode geometry, mass transport and electrochemical kinetic parameters. A curve fitting procedure was used to deduce from the experiments the exchange current density and internal ohmic resistance values according to Equation A3. This fitting procedure assumes a uniform current distribution (i.e. uniform kinetic and mass and charge transport parameter distributions) over the MEA surface corresponding to the average current density. A more realistic approach would have been to consider a non-uniform current density distribution over the cell surface and to integrate the different current values in order to obtain a better estimate of the overall parameters. The possible non-uniform distribution of current densities is investigated further in this paper by magnetic field measurement.

Figure 7 shows the good overall agreement obtained between measurements and predictions on the basis of the parameters in Table 1. The oxygen exchange current density and the resistance also agree with literature data. On the other hand, the estimated hydrogen exchange current density value is rather small compared with values found in the literature. Nevertheless, in the case of low polarisation, a discrepancy in the values was observed. In fact, a Tafel kinetic model is not valid for low polarisation; a Butler Volmer equation would be more appropriate.

The estimated electrochemical and mass transport parameters shown in Table 1 were used to simulate the impedance diagram along the polarisation curve.

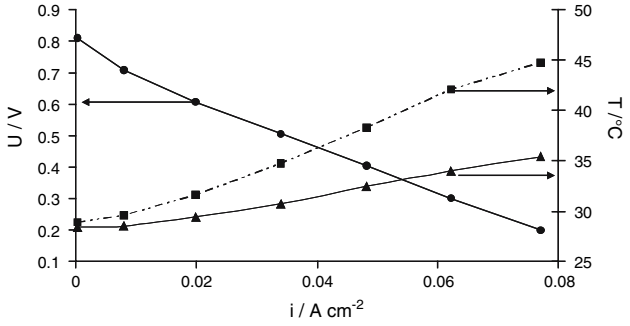

Fig. 5. Cell potential vs. current density curve (•) and corresponding highest (■) and lowest (▲) measured fuel cell temperatures (catalyst loading: 0.3 mg cm^{-2}).

Experimental and simulated impedance diagrams obtained for $i = 0.03$ A cm^{-2} are shown in Figure 8. The proposed model also provides a suitable description of the cell impedance diagrams along the polarisation curve in a medium frequency domain (1–100 Hz) where the contribution of electrochemical reactions occurs.

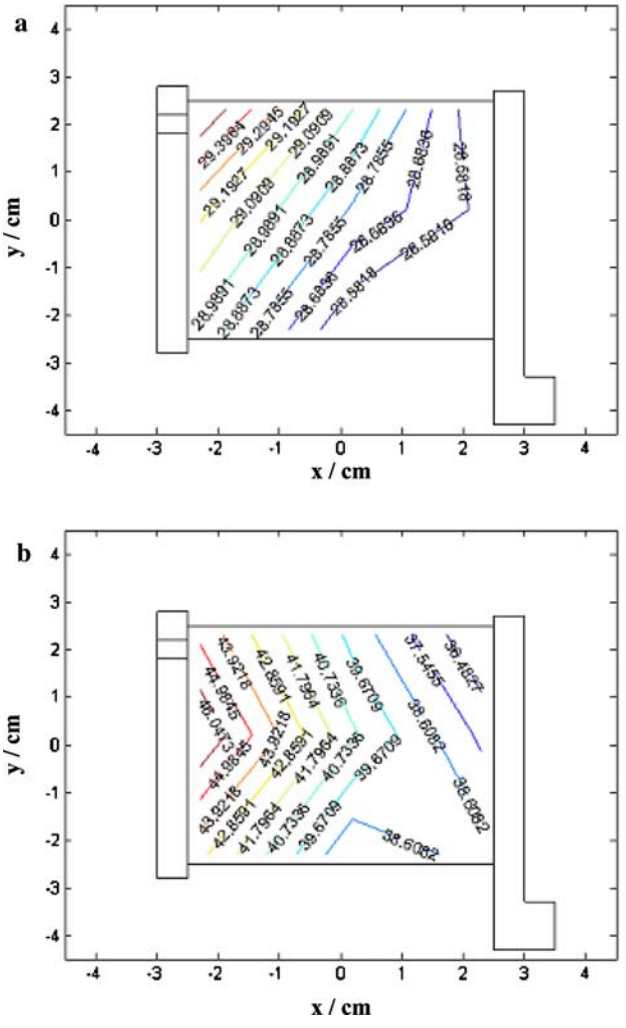

Fig. 6. Temperature (°C) distributions along the cathode surface area at low (a): $i = 0.01$ A cm^{-2}, ($U = 0.7$ V) and high (b): $i = 0.077$ A cm^{-2}, ($U = 0.2$ V) current densities (catalyst loading: 0.3 mg cm^{-2}).

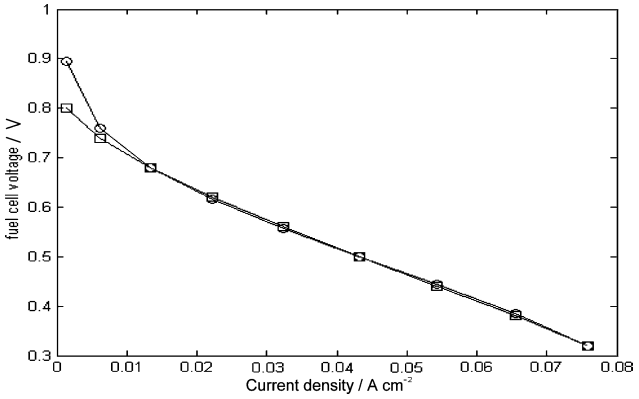

Fig. 7. Example of polarisation fitting using a simple model. □: experimental polarisation; ○: fit (catalyst loading: 0.3 mg cm^{-2}).

Table 1. Electrochemical characteristics deduced from the curve plotted in Figure 7

Hydrogen exchange current	0.05 A
Oxygen exchange current	0.004 A
Electrolyte resistance	0.08 Ohm
Cathode limiting current value	2.2 A

Note that a double layer capacitance equal to 50 F m^{-2} was used. However, discrepancies clearly appeared for low (< 1 Hz) and high frequency (> 100 Hz) domains. The values of internal resistance deduced from the polarisation curves and impedance diagrams were significantly different. Behaviours at high and low frequencies may be, respectively, attributed to the double layer charging process and to water management. According to PEMFC electrochemical behaviour, processes characteristic of oxygen reduction and hydrogen oxidation could appear on the impedance spectra. Theoretical approaches predict that these electrochemical processes should split the PEMFC impedance into two arcs corresponding to oxygen reduction and hydrogen oxidation kinetics. Neither of these arcs can be seen separately in the experimental impedance results pre-

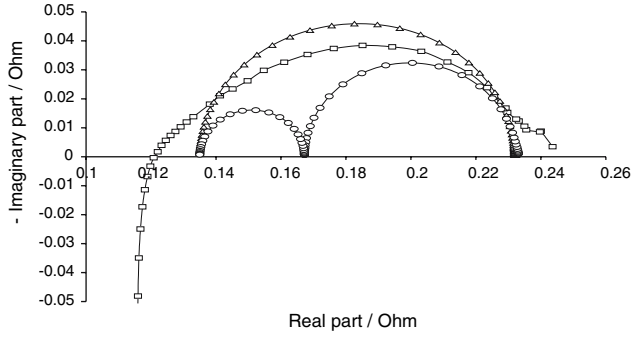

Fig. 8. Experimental (□), simulated (△) and simulated with a difference of two magnitude orders of the double layer capacitance (○) impedance diagrams of a self-breathing PEM fuel cell (catalyst loading: 0.3 mg cm^{-2}).

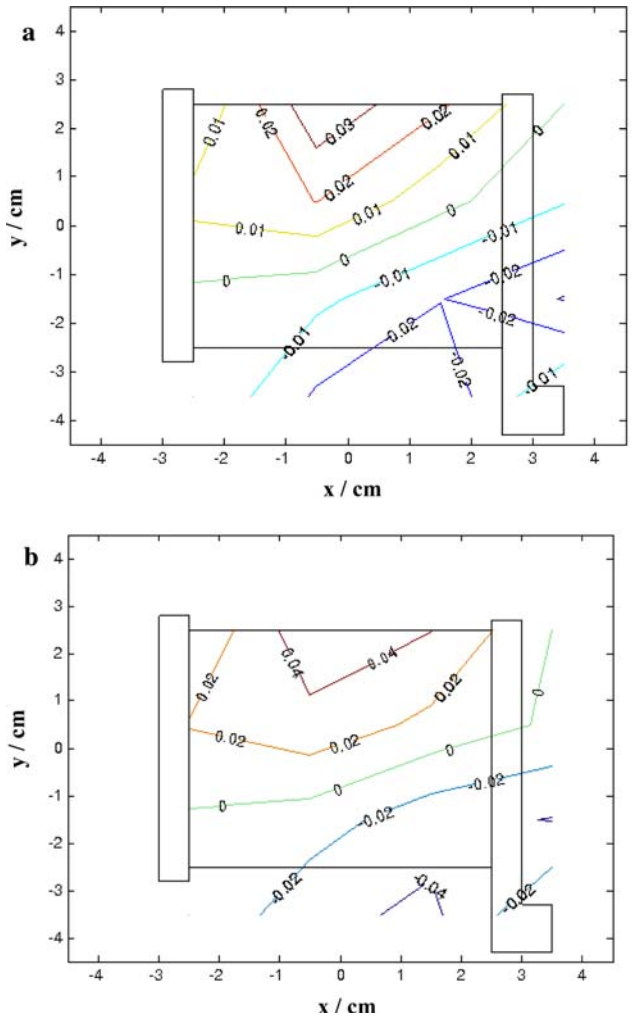

Fig. 9. Calculated current density on the fuel cell (a: 0.066 A cm^{-2} and b: 0.12 A cm^{-2}).

sented in Figure 3. This is due to a masking effect of the high value of the double layer capacitance at the electrode/electrolyte interface. The separation of the charge transfer resistance arc is only possible when considering a smaller double layer capacitance for the anode in order to simulate the PEMFC impedance diagrams. In order to distinguish the anodic and cathodic contributions, the double layer capacitances of the electrodes were fixed, with a difference of two orders of magnitude. Decreasing the double layer capacitance leads to a shift of the anode charge transfer arc in the frequency domain towards higher frequencies. In such conditions, these contributions are clearly distinguished [13] and two semi-circles appear, corresponding to charge transfer resistances. Note that mass transport contributions are not exhibited at low current density (i = 0.03 A cm^{-2}).

Magnetic field measurements (Figure 4) can be used to calculate current density distribution over the cathode surface on the basis of Maxwell's law (Equation 4) as shown in Figure 9. This approach predicts a non-uniform current distribution with higher current densities close to the current collectors and the gas inlet. Nevertheless, the estimated current density remains low compared with the mean current density (0.06 A cm^{-2} and 0.12 A cm^{-2}). This attenuation is mostly due to the distance between the electrode coordinate (z = 0) and the sensor measurement coordinate (z_1 = 5 mm), which is not taken into account in Equation 4.

A more accurate evaluation of the field induced near the cell is provided by the Biot–Savart law which takes into account all the current sources, the membrane thickness and the sensor coordinate. This equation is useful for an analytical study of the complete configuration of the cell electrical connectors and collector grids.

In order to plot more understandable curves, Figure 10 shows the analytical values of induction created exclusively by the current distribution in the membrane. Calculations were performed with Matlab® using Equation 5 for three different distribution cases:

- case "a": the current is assumed to be uniformly distributed on the membrane;
- case "b": current density is assumed to increase from 0 to a maximum density when the y coordinate increases (note that the total current I_{total} is unchanged and remains the same as in case "a");
- case "c": current density is assumed to increase from 0 to a maximum density when the x coordinate increases and the y coordinate decreases (note that the total current I_{total} is unchanged and remains the same as in case "a").

Vector fields of induction B present an eye pattern in cases "a" and "b" and two eye patterns in case "c" (Figure 11). For case "b" the centre of the eye is shifted – compared with case "a" – towards higher current densities close to the hydrogen gas inlet.

Figure 10 presents normalised induction values (with a constant equal to $4\pi/\mu_0$ which is equal to 10^7). Comparison of the calculated induction components (Bx and By) for case "c" (Figure 10) with measurements (Figure 4) shows similar patterns, indicating a similar distribution of currents in the experimental fuel cell. This current distribution is in agreement with the temperature profiles, which exhibit heat sources close to the current collectors, and highlights the effects of the electrical collectors and connectors.

5. Conclusions

This study presents a combination of experimental and theoretical studies devoted to the electrochemical performance a self-breathing PEMFC. Experimental impedance spectra exhibited just one large capacitive arc in the Nyquist plane plot. This arc was created by

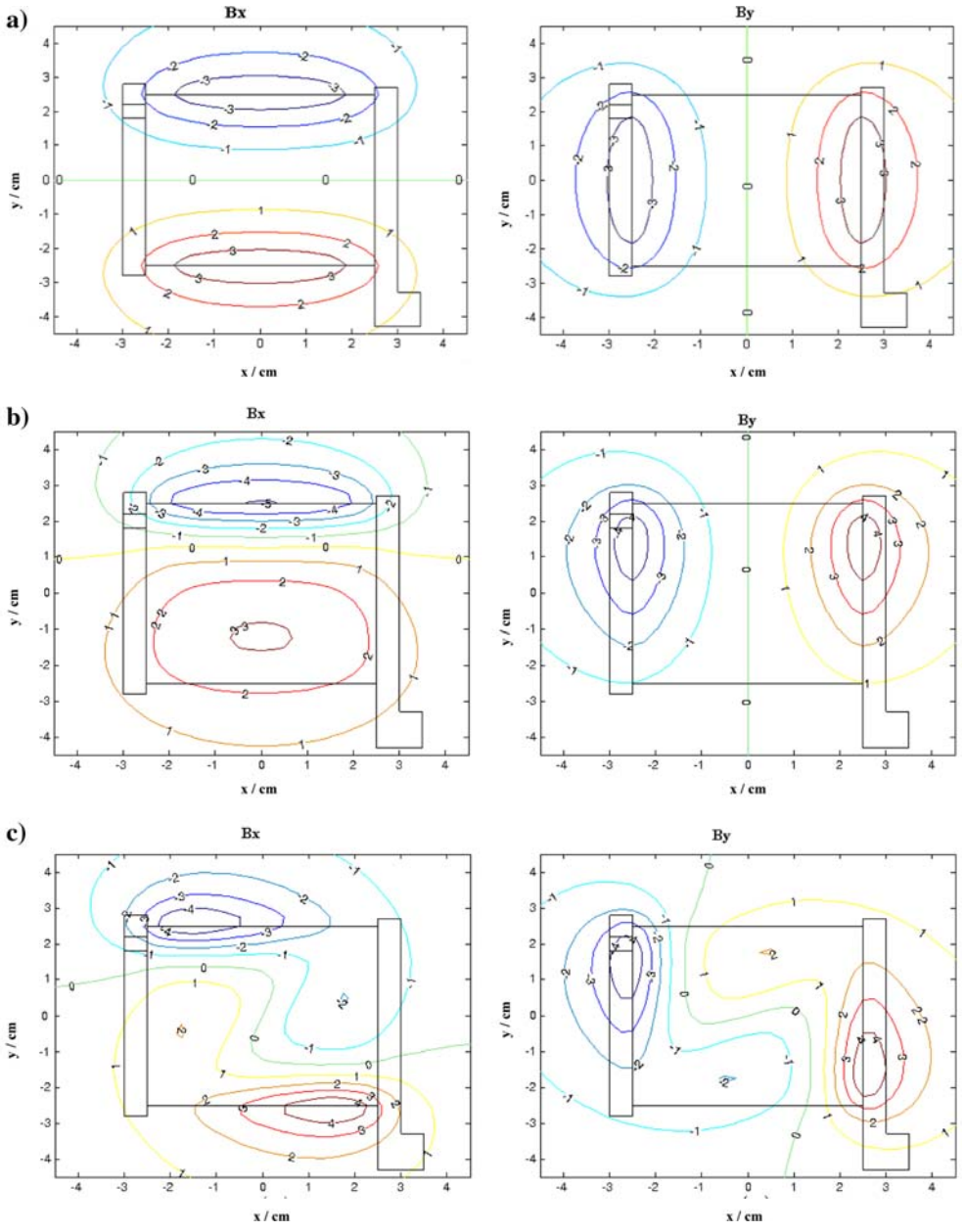

Fig. 10. Contour plots of magnetic field induced by a uniform current density (a), contour plots of magnetic field for a current density increasing with abscissa y (b), contour plots of magnetic field for a current density increasing with the absolute value of (x–y) (c).

intimately intertwined anode and cathode charge transfers attributable to the masking effect of the high double layer capacitance value. A simple model of a self-breathing PEMFC has thus been proposed to predict impedance diagrams. The model proved to be useful for analysing the influence of each electrode.

Finally, locally induced magnetic field and temperature measurements highlighted the heterogeneous distribution of the current densities over the fuel cell area. This distribution demonstrates the influence of cell geometry and current collector location. Inverse calculation of local density from magnetic field values was performed but it would be interesting to use three-axis induction measurements in order to increase their accuracy before computing local current densities.

6. Annex

The flooded agglomerate model for the PEMFC active layers can be used to describe the real current density within the active layer as a function of Thiele's modulus (U_i) and the gas concentration in the gas pores of the active layer [11]. Assuming a Tafel kinetics law, the flux continuity equation at the interface between the gas backing layer and the active layer enables us to express the local current density j from the limiting current density (j_{lim}) as:

$$j = \gamma \cdot j_{0,i} \cdot \exp\left(\frac{2,3}{b_i}\eta_i\right) \cdot \left(1 - \frac{j}{j_{\text{lim},i}}\right) \cdot \frac{\tanh(\sqrt{U_i})}{\sqrt{U_i}} \qquad (A1)$$

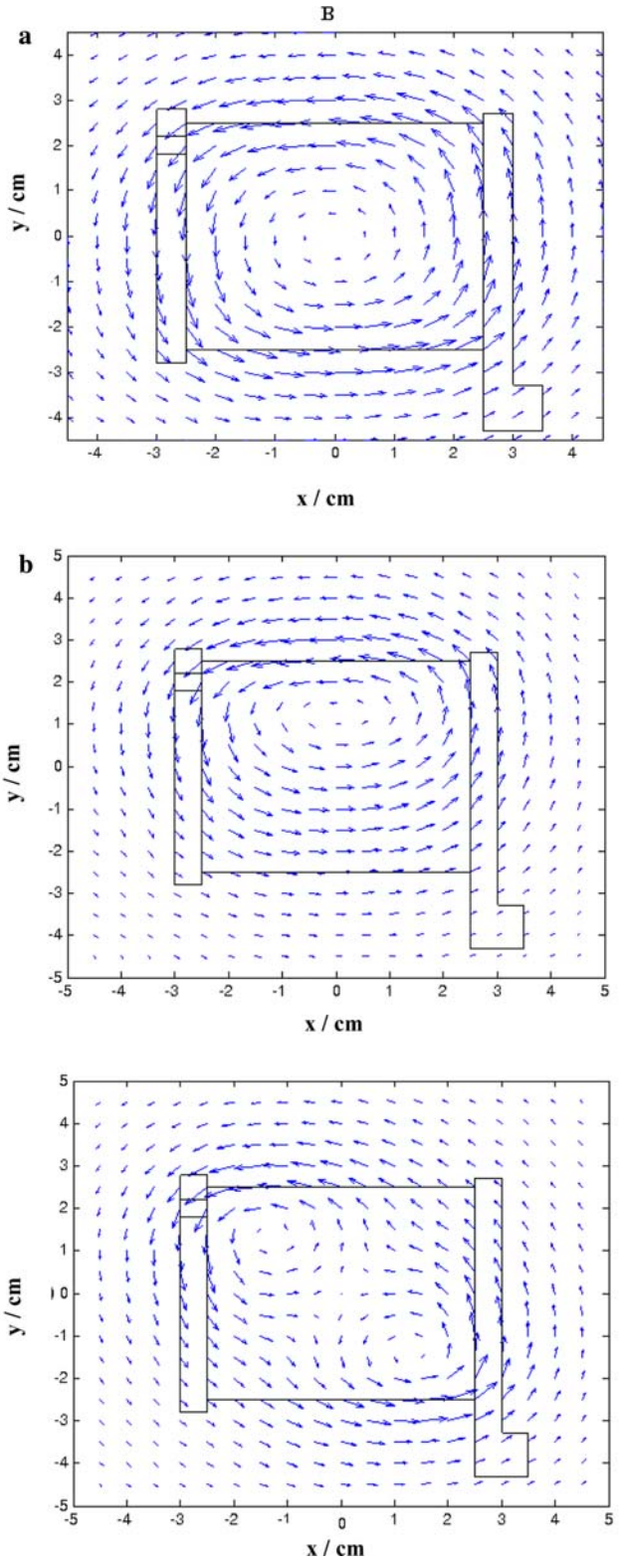

Fig. 11. Vector fields of induction B induced by a uniform current density (a), vector fields of induction B of magnetic field for a current density increasing with (y) (b). Vector fields of induction B of magnetic field for a current density increasing with the absolute value of (x–y) (c).

where γ is the roughness factor (−), j_0 the exchange current density (A m^{-2}); b the Tafel slope (V dec^{-1}), η the overpotential (V) and i an index referring to the anode (a) or cathode (c). Note that Thiele's modulus (U_i), the ratio of the kinetics rate to the diffusion flux density, is given by:

$$U_i = \frac{\gamma \cdot L j_{0,i} \cdot \exp\left(\frac{2,3}{b_i}\eta_i\right)}{n_{\mathrm{ei}} F D_i^{\mathrm{AL}} c_{r,i}} \qquad (A2)$$

L being the agglomerate half-thickness (m), n_{ei} the total number of exchanged electrons, F Faraday's constant (96,500 C mol^{-1}), $D_{\mathrm{i}}^{\mathrm{AL}}$ the effective diffusion coefficient (m^2 s^{-1}).

For a given current density distribution j, the cell voltage U_{cell} may be calculated by solving Equation A2 for oxygen and hydrogen species and from the internal resistance (R_{int}) of the cell:

$$U_{\mathrm{cell}} = 1.23 - \eta_{\mathrm{a}}(j) + \eta_{\mathrm{c}}(j) - R_{\mathrm{int}} \cdot j \qquad (A3)$$

The physical model used to obtain the governing equations for the ac PEFMC impedance is based on a previous two-dimensional model [14]. In the frequency domain, restricted diffusion impedance, assuming a Fick's law, approximately describes the contribution of mass transport within the gas backing layer. The faradic impedance Z_{f} of the gas diffusion electrode is then obtained from a simplified solution, including only the contribution of mass transport in the gas phase:

$$Z_{\mathrm{fi}} = \pm\frac{1}{\gamma_i\left(\partial j_{\eta,i}\right)} + \frac{\partial j_{\mathrm{c},i}}{\left(\partial j_{\eta,i}\right)} \cdot \left(\frac{\delta}{n_{\mathrm{ei}} F D_i^{\mathrm{GBL}}} \cdot \frac{\tanh\sqrt{p\tau_i^{\mathrm{GBL}}}}{\sqrt{p\tau_i^{\mathrm{GBL}}}}\right)$$
$$\text{and } \tau_i^{\mathrm{GBL}} = \frac{\delta^2}{D_i^{\mathrm{GBL}}} \qquad (A4)$$

where δ is the gas backing layer thickness (m), D_i^{GDL} the effective diffusion coefficient (m^2 s^{-1}), p the Laplace variable, τ_i^{GDL}, the time constant (s). The two derivation terms are defined as: $\partial j_{\eta,i} = \partial j/\partial\eta$, $\partial j_{\mathrm{c,i}} = \partial j/\partial c$.

The complete description of the electrode impedance still requires consideration of the double layer capacitance C_{dl}. Although physically distributed throughout the agglomerate, the double layer capacitance can be separated from the agglomerate region from a mathematical point of view if ohmic drop limitation in the active layer is ignored [11]. The local anode or cathode impedance Z_i is then calculated by considering the faradic impedance and the double layer capacitance (C_{dl}) in parallel:

$$Z_i = \frac{1}{\frac{1}{Z_{\mathrm{fi}}} + p\gamma C_{\mathrm{dl}}} \qquad (A5)$$

while the impedance of the Membrane Electrode Assembly, which is simply the sum of internal resistance and electrode impedances, is obtained from an equivalent electrical circuit as proposed by Wagner [10]:

$$Z_{\mathrm{cell}} = Z_{\mathrm{a}} + R_{\mathrm{i}} + Z_{\mathrm{c}} \qquad (A6)$$

Table 2. Input parameters used for simulation

	Anode	Cathode
γ: Roughness factor (–)	100	100
δ: Diffusion layer thickness (m)	1000×10^{-6}	1000×10^{-6}
L_{AL}: Active layer thickness (m)	20×10^{-6}	20×10^{-6}
$2 \times L$: Agglomerate thickness (m)	1×10^{-6}	1×10^{-6}
ε^{GBL}: Gas backing layer porosity	0.5	0.5
ε^{AL}: Active layer porosity	0.5	0.5
b: Tafel slope (V/dec)	0.06	0.12
n_e: Total number of exchanged electrons	2	4
D^{GBL}: Effective diffusion coefficient in the GBL ($m^2\ s^{-1}$)	$2.2 \times 10^{-4} \times (\varepsilon^{GBL})^{1.5}$	$2.2 \times 10^{-5} \times (\varepsilon^{GBL})^{1.5}$
D^{AL}: Effective diffusion coefficient in the AL ($m^2\ s^{-1}$)	$10^{-9} \times (\varepsilon^{AL})^{1.5}$	$10^{-9} \times (\varepsilon^{AL})^{1.5}$
P: Gas pressure (bar)	1.2	1
T: PEMFC temperature (°C)	30	

Note that Table 2 shows the values of the input parameters for the simulation provided by the literature [14].

References

1. E. Passalacqua, G. Squadrito, F. Lufrano, A. Patti and L. Giorgi, *J. Appl. Electrochem.* **31** (2001) 449.
2. J.R. Selman and Y.P. Lin, *Electrochim. Acta* **38** (1993) 2063.
3. V.A. Paganin, C.L.F. Oliveira, E.A. Ticianelli, T.E. Springer and E.R. Gonzalez, *Electrochim. Acta* **43** (1998) 3761.
4. T.J.P. Freire and E.R. Gonzales, *J. Electroanal. Chem.* **503** (2001) 57.
5. G. Maggio, V. Recupero and C. Montegazza, *J. Power Sources* **62** (1996) 167.
6. M. Nopponen, T. Mennola, M. Mikkola, T. Hottinen and P. Lund, *J. Power Sources* **106** (2002) 313.
7. J. Stumper, S.A. Campbell, D.P. Wilkinson, M.C. Johnson and M. Davis, *Electrochim. Acta* **43** (1998) 3773.
8. D. Candusso, J.P. Poirot-Crouvezier, B. Bador, E. Rulliere, R. Soulier and J.Y. Voyant, *Eur. Phys. J. Appl. Phys.* **25** (2004) 67.
9. O. Chadebec, J.L. Coulomb, L.L. Rouve, J.P. Bongiraud, G. Cauffet and P. Le Thiec, *IEEE Trans. Magn.* **38** (2002) 1005.
10. N. Wagner, *J. Appl. Electrochem.* **32** (2002) 859.
11. T.E. Springer and I.D. Raistrick, *J. Electrochem. Soc.* **136** (1989) 1594.
12. M. Eikerling and A.A. Kornyshev, *J. Electroanal. Chem.* **475** (1999) 107.
13. Y. Bultel, L. Geniès, O. Antoine, P. Ozil and R. Durand, *J. Electroanal. Chem.* **527** (2002) 143.
14. M. Bautista, Y. Bultel and P. Ozil, *Chem. Eng. Res. Design Part A* **82(A7)** (2004) 907.